

Automotive Radar Target List Simulation based on Reflection Center Representation of Objects

Markus Bühren and Bin Yang
Chair of System Theory and Signal Processing
University of Stuttgart, Germany
www.LSS.uni-stuttgart.de

Abstract—In various signal processing areas, simulated data is used in the first phase of algorithm development. Simulated data has the advantage that it provides an exact reference allowing to compute objective error measures. Further, no time-intensive measurement campaigns are necessary. In the field of automotive radar, however, real data is used from the beginning. This is due to the high complexity of the underlying electromagnetic wave model. In this paper, we present a model for the simulation of automotive radar target lists – i.e. the measured distance, angle, relative speed and amplitude of detected targets – that is much less demanding in terms of implementation and computation effort than, for example, a finite-element or ray-tracing model.

I. INTRODUCTION

Simulated data is used in the first step of algorithm development in many signal processing areas. For example, when developing algorithms for time-difference of arrival (TDOA) estimation of audio signals, one would start with artificially shifted and perturbed signals instead of signals recorded in a real environment. If the algorithm works well with simulated data, real measurement data are used for refining and verifying.

The first argument that speaks for the use of simulated data is that it provides an exact reference. In the example of TDOA estimation, it is possible to compute the estimation error easily and exactly. When using real data, however, there is no exact reference available in the most cases. Algorithms can only be evaluated quantitatively by the sight of lots of test scenarios.

The second argument against working solely with real data is the time and equipment needed for measurement campaigns. For a comparably simple automotive radar application like the adaptive cruise control (ACC), it might be possible to cover a large part of relevant scenarios with test runs. For more advanced applications like intersection assistance, on the other hand, the effort for the creation of a set of representative test scenarios will be unbearable. When working on systems that require more than one vehicle to be equipped with radar in the future, the costs will increase even more.

Despite these facts, real radar data is used from the beginning of algorithm development in the automotive radar field. The reason for this is the high complexity of the underlying physical model. Even if the electromagnetic waves follow comparably simple rules, modeling radar objects like vehicles or pedestrians on the one hand and the radar sensors itself on the other hand is very complicated. Three-dimensional models consisting of a huge number of elements would be necessary to simulate radar signals when building a simulation model on a very low physical level.

Our simulation of radar signals is aimed to serve as a tool for the development of radar signal processing algorithms that start with the radar target list as input data, i.e. tracking or data fusion algorithms. By restricting the field of use of the simulation to the development of algorithms of that class, we are able to build a simulation that is much simpler than a finite-element model on the level of Maxwell's equations or a ray-tracing model. Simulating radar signals on a very low level would mean a lot of overhead in terms of implementation

effort and computation time, as we are only interested in the higher-level radar target list as the desired simulation output.

The motivation for our new approach are the observations of radar experts and our experience with real automotive radar data. We are abstracting vehicles and obstacles in a very simple but accurate way by a small number of reflection centers, which is sufficiently detailed for a realistic simulation of the data we need. Note that in a simulation which is used as a tool for algorithm development, not every physical effect has to be considered. Effects that will not be especially accounted for in the algorithms do not have to be reproduced. The resulting simulation is computationally very undemanding and able to run nearly in real-time on a standard 3 GHz PC.

In section II, the motivation for the new approach of abstracting vehicles and other objects is presented. With this abstraction and a traffic scene (positions and speeds of several objects), an ideal radar target list in terms of distance, angle and relative speed can be computed. The ideal target list is then transformed into a realistic one by applying a specific sensor model, as described in section III. The target list simulation principle is summarized in section IV, before real radar target lists are compared to simulated ones in section V. Possible ways of improving the simulation are finally given in section VI.

II. VEHICLE MODEL

A. Motivation

We start this section by explaining our motivation for the new approach of representing objects. In the following figures, radar target lists recorded on test runs are shown in bird's eye-view. The observing vehicle (on the left) is equipped with two Tyco Electronics M/A-Com 24 GHz short range radar sensors (SRR), as described in [1]. The principal beam width of 70° is indicated. The detected targets (positions determined by measured distance and relative angle) are shown by circles (right sensor) and stars (left sensor). The lines next to the target indicators represent the measured relative speed. The lines always point to or away from the sensors, as the radial speed is measured. The line length is proportional to the measured speed. The contour of the target vehicle was inserted manually.

Figures 1 and 2 show that the corners and – at small distances – the wheel houses appear in the target list. This motivates the introduction of so-called *point reflection centers* at the four vehicle corners and the four vehicle houses. Of course, not every point reflector will cause a target list entry, for example, when the target is illuminated from the opposite side. In order to consider this fact, we assign a visibility range to each point reflector. Fig. 3 shows the contour of a vehicle from the top and the corresponding eight point reflection centers with their visibility ranges (labeled A...H).

Fig. 4 demonstrates that point reflectors alone are not sufficient for modeling a vehicle realistically. The figure is a snapshot of a situation where the target vehicle was moving perpendicular to the non-moving observer. The target positions are straight ahead in the

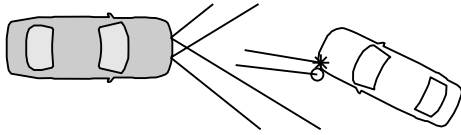


Fig. 1. Target vehicle corner

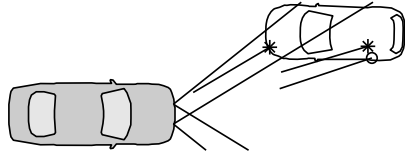


Fig. 2. Target vehicle corner and wheel house

main view direction of the two sensors. The measured relative speed is zero, thus there are no lines indicating the measured speed visible. The target position stays fixed for a number of time instances even if the target is moving, as you can see in Fig. 5, where the measured y-positions of the right radar sensor are plotted over the time. After the first detection (which is delayed due to sensor-internal tracking, see section III-E), the measured y-position stays constant, as the vehicle side is in view. As the target vehicle moves on, after some seconds only the rear-right corner of the vehicle is detected, which corresponds to a point reflector in our model. Now the measured y-position decreases linear.

This behavior can easily be modeled by introducing so-called *plane reflectors* to the model. We define a plane reflector as a circle sector, or, seen in three dimensions, as a part of the surface of a circular cylinder with its axis parallel to the z-axis. The plane reflectors are drawn as thick lines in Fig. 3.

B. Reflection center visibility

Instead of defining a visibility region with sharp boundaries to each point reflection center, we use a continuous visibility function depending on the impinging angle. This function has a value of one in the angular region where it can be seen best and decreases until zero in regions where it is impossible that the radar sensor receives any reflected energy. The visibility range introduced above corresponds to the part of the visibility function that is greater than zero. In Fig. 6, the visibility functions of the eight point reflection centers in Fig. 3 are shown over the impinging angle which is measured with respect to the longitudinal axis of the target vehicle. The circle markers highlight the resulting function values in a situation where the radar sensor

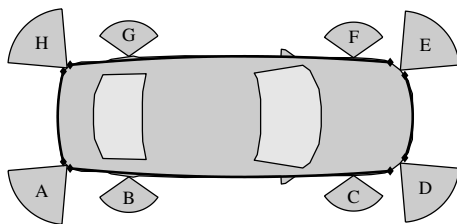


Fig. 3. Vehicle reflection model

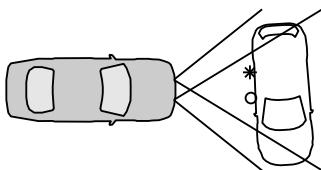


Fig. 4. Target vehicle side

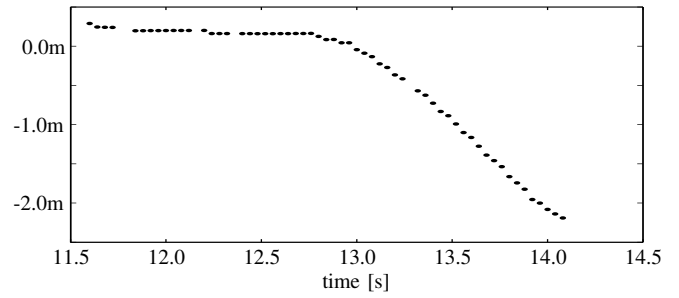


Fig. 5. Measured y-positions of vehicle passing perpendicular

is placed in a distance of about three meters right-behind the target vehicle.

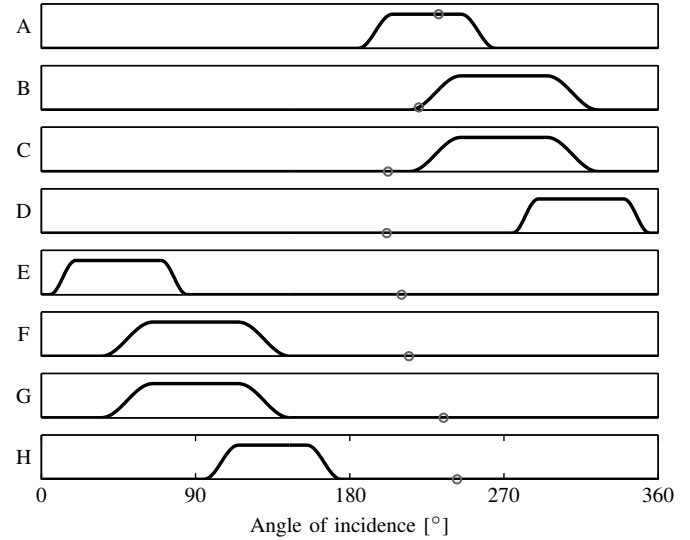


Fig. 6. Visibility functions

The determination if a point reflection center can possibly be detected by a radar sensor is illustrated schematically in Fig. 7. When the radar sensor is in position 1, it is outside the angular visibility region of the point reflection center, which is thus invisible to the radar. In contrast, the visibility range of the point reflector covers sensor position 2; a radar sensor at this position could possibly detect the reflector.

When the radar sensor is in position 1 in Fig. 7, the plane reflector is illuminated perpendicular and can thus be detected. The resulting reflection point is computed as the intersection point of the connection between sensor position and circle center with the circle sector defining the plane reflector. The reflection point computed for sensor position 2 is invalid because does not lie on the plane reflector.

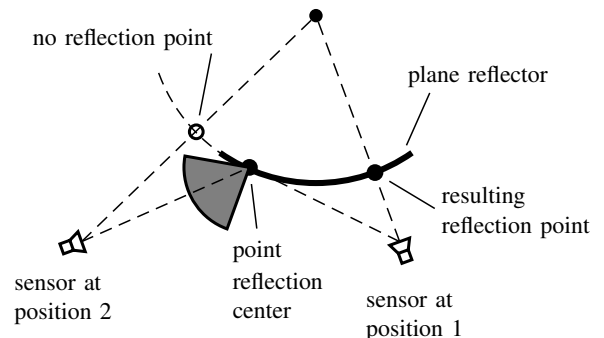


Fig. 7. Visibility evaluation

However, a point reflection center or a plane reflector that passes this visibility check does not cause a target list entry in any case; the final decision is later done based on the simulated amplitude.

C. Radar cross section

For both types of reflectors, an important simulation parameter is the radar cross section. This allows the simulation of the radar amplitude and the determination if the returned radar echo is strong enough to cause a detection or not (see section III-B).

In the case of a plane reflector, the radar cross section is set to a constant independent of the impinging angle. In contrast to this, we use a scaled version of the visibility function to compute the radar cross section of a point reflection center depending on the impinging angle α .

In each case, reasonable values for the radar cross section have to be derived by inspection of real radar data. Different kinds of planes, for example vehicle front end, rear end and side, will all result in a radar echo of different amplitude. As well, the amount of radar echo to be expected from the wheel houses will differ from vehicle to vehicle. In Fig. 3, the radius of the circle sectors is proportional to the radar cross sections of the corresponding point reflection centers.

With this concept of point reflection centers and plane reflectors, vehicles as well as simpler objects (e.g. reflecting poles, guide boards) and more complicated objects (e.g. a truck with trailer) can sufficiently be modeled. In all cases, the necessary parameters have to be derived by inspecting real radar data. The effort for the collection of real data, however, is much smaller in comparison to the usual way, where algorithm development is done solely based on real data. The overall number of elements, in our case reflection centers, is orders of magnitude lower than it would be necessary in a finite-element field simulation or ray-tracing model.

III. RADAR SENSOR MODEL

With the representation of vehicles and objects as described so far, we are able to transform a traffic situation around the observing vehicle into an ideal target list in terms of distance, angle, relative speed and radar cross section. Every reflection center that has passed the visibility test has its own corresponding entry in the ideal target list. In this section we describe our model of the before mentioned SRR radar sensors [1] which turn the ideal target list into a realistic one. As we do not have insight into the sensor-internal processing, we have to make assumptions in some places.

A. Measurement errors in distance and relative speed

As the experience with real radar data shows, measurement errors in distance and relative speed can sufficiently be modeled as white Gaussian noise. Fig. 8 shows the histogram of distance measurements with a corner reflector as the target (The histogram of the relative speed measurements looks similar and is thus omitted here). The fitted Gaussian density curve shows good coincidence. Following this observation, we simulate those errors by adding pseudo-random noise to the computed ideal values. The appropriate noise variance is the lower the stronger the target response is. In order to consider this fact, the radar amplitude is simulated as shown in the next section.

B. Radar amplitude simulation

For the radar amplitude simulation, we have examined the amplitude of the front of an Opel Vectra as our reference target in various test runs. Fig. 9 shows the amplitude in one test run over the distance to the target. As we are solely interested in the influence of the front

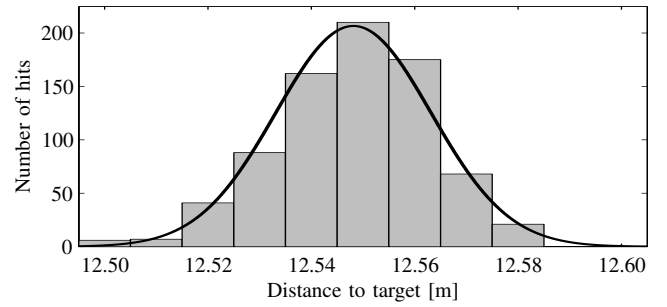


Fig. 8. Histogram of distance measurements

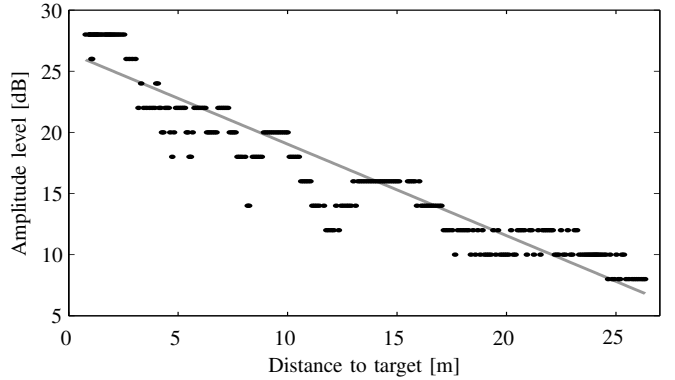


Fig. 9. Radar amplitude of the front of an Opel Vectra

plane reflector of the reference vehicle, only those detections with the minimum distance in every cycle were used.

First of all we note that the $1/R^4$ -law the radar amplitude emerging from the radar equation does not hold in this case. The reason for this is that the view conditions – and with that the radar cross section – change significantly with changing distance to the target. The $1/R^4$ -law is only true if all involved parameters except the range are constant. In our measurements, we observe a nearly linear dependency between the distance and the amplitude in dB, as indicated by the trend line in Fig. 9. Following this observation, we model the range-dependent part of the radar amplitude of our reference reflector as

$$L\{A_{\text{ref}}^R(R)\} = \left(26.5 - 0.75 \frac{R}{\text{m}}\right) \text{ dB} \quad (1)$$

with the level of the amplitude A in dB related to a reference A_0 , $L\{A\} = 20 \log_{10} |A/A_0|$ dB, and the distance to the target, R . As the resulting amplitude also depends on the antenna pattern $A^\phi(\phi)$ (normalized to 1 in the main direction, see section III-D), the resulting amplitude for the reference reflector is computed as

$$A_{\text{ref}}(R, \phi) = A_{\text{ref}}^R(R) \cdot A^\phi(\phi). \quad (2)$$

with the target angle ϕ .

An *equivalent radar cross section* (ERCS) of 1 is arbitrarily assigned to the reference reflector (note that we do not have any information about the relation between the returned amplitude level in dB and the received power in Watt and thus use normalized numbers here). The equivalent radar cross sections of other reflection centers have to be derived by inspection of real radar measurements. In the case of a point reflection center, we use a scaled version of the visibility function that was introduced before. Finally, the amplitude generated by an arbitrary reflector k is computed by multiplying the amplitude of the reference target with the equivalent radar cross section of the reflector:

$$A_n(R_n, \phi_n) = A_{\text{ref}}(R_n, \phi_n) \cdot \text{ERCS}_n(\alpha_n) \quad (3)$$

With help of the simulated amplitude, we are able to determine if a reflection center would be detected by a radar sensor or not. This is done by computing the resulting amplitude for each resolution cell (see the next section for the definition of a resolution cell). If this amplitude is lower than 6dB (the lowest returned amplitude of any target in our measurements), no target is returned in that resolution cell.

The amplitude shown in Fig.9 shows slight decays, e.g. at a distance of about 8m and 12m. These are due to multipath and interference effects. A multipath-model could help to make the amplitude simulation even more realistic.

C. Limited resolution

As a real radar sensor has limited resolution capabilities, not every reflection center will cause its own target list entry. All reflection centers inside one *resolution cell* – in our case a cell in the dimensions distance and relative speed – will superimpose and cause a single entry.

In order to simulate this behavior, we could build a model for the form of returned radar pulses, the sampling of overlapping pulses and so on. However, this would require a number of assumptions as we do not know about all internal details of the radar sensors. Instead, we decided to use a much simpler clustering approach which needs only assumptions about the resolution cell size (we assume $30\text{cm} \times 0.5\text{m/s}$). The clustering algorithm starts with the strongest reflection center, which defines the center of the first resolution cell. The sum of the radar amplitudes of all reflection centers inside this cell gives an upper threshold for the resulting radar amplitude, A_{cell}^u . If this value is lower than the detection threshold mentioned before, no target list entry will result.

As we expect that reflection centers with a high amplitude $A_n(R_n, \phi_n)$ will have a higher impact on the resulting distance and speed measurement values, d_{cell} and v_{cell} , than those with lower amplitudes, we approximate the superposition of radar energy at the receiving antenna by weighted sums for the resulting values for the current cell:

$$d_{\text{cell}} = \sum_n d_n w_n \quad , \quad v_{\text{cell}} = \sum_n v_n w_n \quad (4)$$

with

$$w_n = A_n(R_n, \phi_n) / \sum_n A_n(R_n, \phi_n) \quad (5)$$

The clustering algorithm now proceeds with the reflection center with the highest amplitude among the remaining ones and so.

D. Angle estimation principle

In contrast to the simple addition of pseudo-random noise in the case of distance and speed measurements, a realistic simulation of angle measurement errors requires to take the angle estimation principle into account. A particular effect that would otherwise hard to be modeled is shown in Fig. 10. Here two vehicles are in the view field of the radar sensor but only one target is returned in the center. The reason for this effect will become clear in the following.

The monopulse principle implemented in the radar sensors we used takes advantage of two receive antennas with different antenna patterns (dashed lines Fig. 11). We approximate the so-called *sum* and *delta* patterns described in [1] by the antenna pattern of an array of two half-wavelength long dipoles spaced by a half wavelength λ (solid lines in Fig. 11). Exciting both dipoles in phase results in the sum pattern, while a phase shift of π results in the delta pattern. The resulting complex pointers, neglecting factors depending on elevation angle and target distance, are $(\Sigma$: sum pattern, Δ : delta pattern) [2]:

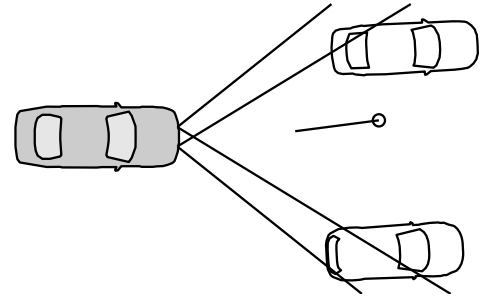


Fig. 10. Angle estimation error in one resolution cell

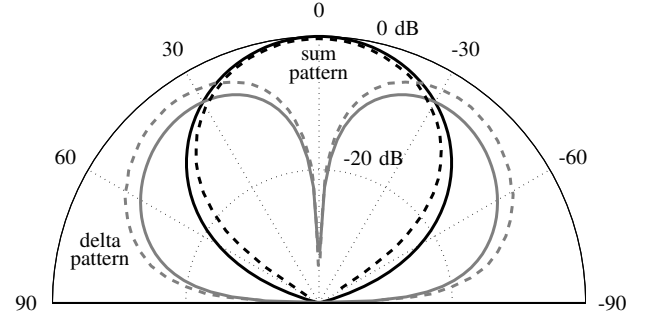


Fig. 11. Sum and delta antenna patterns

$$H_{\Sigma}(\phi) = \text{si}\left(\frac{\pi L}{\lambda} \sin(\phi)\right) \cos(\phi) \cdot \frac{1}{2} \left(1 \pm \exp(j\pi \sin(\phi))\right) \quad (6)$$

The magnitude of the sum pointer is used as the antenna pattern $A^{\phi}(\phi)$ in equation (2). The detection area for different values of the equivalent radar cross section ERCS, which results with equations (1)-(3) and the detection threshold of 6dB, is illustrated in Fig. 12.

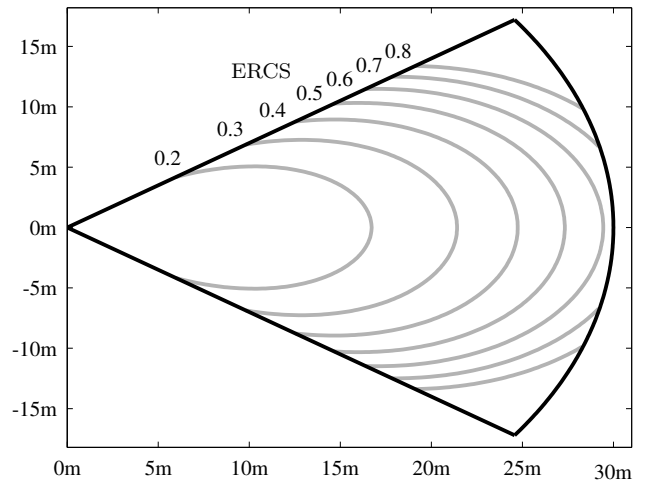


Fig. 12. Visibility area for different ERCS values

For the angle estimation, the so-called *additive sensing ratio*

$$\text{ASR}(\phi) = \frac{|H_{\Delta}(\phi)| - |H_{\Sigma}(\phi)|}{|H_{\Delta}(\phi)| + |H_{\Sigma}(\phi)|} \quad (7)$$

is used. It is a monotonously increasing function of the absolute angle $|\phi|$ and can easily be inverted numerically by table-lookup or a spline representation. The target angle sign can be determined by the phase difference between sum and delta pulse (see [1] for details).

With the closed-form expression (6), the computed ideal angles of all reflection centers can be transformed into pairs of complex pointers corresponding to the sum and delta antenna patterns. By

weighting these pointers with the distance-dependent part of the simulated amplitude, we consider the fact that a strong target will have more influence on the resulting angle than a weak one. Angle estimation noise is simulated by adding complex Gaussian pseudo-random noise to the resulting sums:

$$H_{\text{cell},\Delta} = \sum_n A_{\text{ref}}^R(R_n) \cdot \text{ERCS}_n(\alpha_n) \cdot H_{\Delta}(\phi_n) + \text{Noise} \quad (8)$$

As the artificial noise is of constant variance and the pointers are weighted by the simulated amplitude, targets with lower amplitude will automatically be subject to higher angle errors. From the resulting two pointers $H_{\text{cell},\Sigma}$ and $H_{\text{cell},\Delta}$, the angle estimation is now straightforward as described in [1].

Considering the angle estimation principle used in the radar sensors, the reason for the angle error in Fig. 10 becomes clear. The radar energy of two targets that are well separated in angle but are in the same resolution cell superimposes at the receiver. As well, the complex pointers are summed up and cause an erroneous angle estimation in the center of both targets.

E. Sensor-internal tracking

In a real radar sensor, a crucial part of the sensor-internal processing is the tracking of the noisy measurements. The tracking is important to smooth the noisy estimations, especially the angle estimations, and to suppress false detections. Due to the tracking, target lists of two consecutive time steps are not independent of each other, as it would be in our simulation as described until now.

Modeling the tracking procedure is a much easier task than finding the optimal tracking parameters in the design of a real radar sensor. While the noise characteristics of real measurements are fixed and the tracking parameters have to be chosen optimally, in the simulation we can modify both the noise characteristics and the tracking parameters in order to yield a realistic model of the radar sensor. Further, in our simulation we do not have to face the problem of false detections, as all simulated reflection centers belong to real targets. However, in order to generate realistic conditions, false detections should be added later as they also occur sporadically in reality.

As in other places before, we do not have any information about the tracking procedure used in the radar sensors and have to rely on assumptions. In our simulation model, we apply a simple linear Kalman filter approach [3]. The state space consists of the same variables as the radar target list, i.e. distance, relative speed, angle and amplitude. The input and measurement noise variances that influence the weighting between the new measurement vector and the measurement prediction are still subject to change and will not be discussed here. A target list entry is returned only if the corresponding track was assigned a minimum number of four or more measurements. This parameter is crucial in a real radar sensor, as a higher number of required measurements results in a better suppression of false detections but also in a longer “reaction time”. In our simulation, however, the parameter is uncritical as we do not have any false detections anyway.

IV. TARGET LIST SIMULATION SUMMARY

In order to provide an overview of the whole simulation process, we summarize all simulation steps in this section. The graph in Fig. 13 visualizes the dependency between the different modules.

1) *Traffic simulation/traffic scene database*: The target list simulation needs a traffic scene consisting of positions and speeds of all vehicles and other objects around the observing vehicle as the starting point. This can either be generated by defining the movement of observer and objects by hand for every time step, or by using a

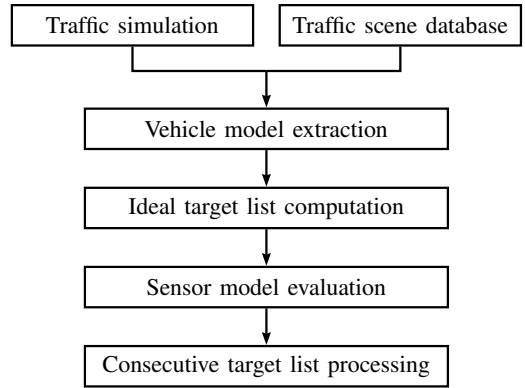


Fig. 13. Hierarchical simulation structure

so-called *microscopic traffic model*, where the reactions of a number of virtual vehicles is simulated (see, for example, [4] [5]). We have realized both possibilities in our existing implementation, as the first method allows the re-simulation of real measurement campaigns as well for building special scenarios, for example in order to observe the angle error effect shown in Fig. 10. The traffic simulation, on the other hand, delivers realistic vehicle speeds and distances in floating traffic and avoids the limitation to only a handful of scenarios in the algorithm development process.

2) *Vehicle model extraction*: The first simulation step is the translation of the traffic scene into reflection centers. A reflection center representation of vehicles and objects appearing in the given traffic scene needs to be provided by an *object model database*. Equivalent radar cross sections and visibility functions have to be derived by inspecting real radar data sets. We expect that the choice of these parameters will not be critical for the later algorithm development. Thus, a moderate amount of measurement data will be sufficient.

For each object, the visibility conditions of all reflection centers are checked as shown in Fig. 7. Only those reflection centers that are in the view field defined by range and beam width of the current sensor are forwarded to the next simulation step.

3) *Ideal target list computation*: The ideal target list in terms of distance, angle and relative speed is computed by means of geometric considerations. Every reflection center that passes the visibility test causes one ideal target list entry.

4) *Sensor model evaluation*: The ideal target list is turned into a realistic one by applying a specific *sensor model*. In the case of the described short-range radar sensor, the sum and delta pointers scaled by the simulated amplitude are computed first. After the clustering procedure that simulates the limited resolution capabilities, the resulting sum and delta pointers of each resolution cell are artificially disturbed by the addition of complex pseudo-random noise; the angle estimation is then done based on the noisy pointers. Errors in distance and relative speed measurements are simulated by adding artificial noise with amplitude-dependent variance. The resulting target list is then forwarded to the internal tracking procedure, which returns the final result of the simulation. This can now be forwarded to the radar target list processing algorithms like target tracking and sensor data fusion.

V. RESULTS

Figures 14-17 contain comparisons between real target lists and their simulated counterparts. The observing vehicle is in each case located on the left of the target vehicle. As stated before, the vehicle contours were set manually into the real data scenarios. The same positions and the corresponding object vehicle representation were used to re-simulate the same scenario. The traces of stars and circles

represent the detections of the two sensors in the last ten time instances.

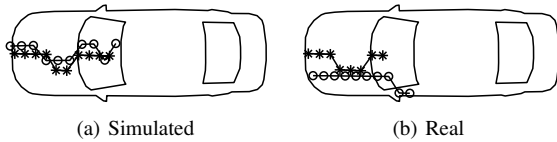


Fig. 14. Real and simulated data in situation 1

Clearly, real and simulated data show similar characteristics in situation 1 (Fig. 14), where the observer faced the front of the Opel Vectra. The distance to the target in the last displayed time instance is about 15m. The results are also satisfactory in situation 2, where the observer approached the corner of the same vehicle (Fig. 15, distance about 12.5m).

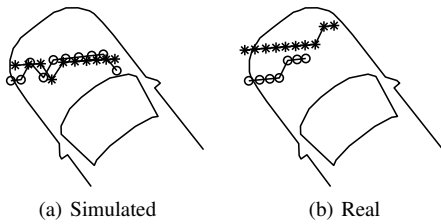


Fig. 15. Real and simulated data in situation 2

In the situation in Fig. 16, the distance between observer and target is about 2.8m. The concept of the front plane reflector is very well approved. In the simulated data, the detections around the left side of the target vehicle windshield are missing. These detections with low amplitude only occur at small distances and are presumably caused by non-ideal focusing in elevation direction.

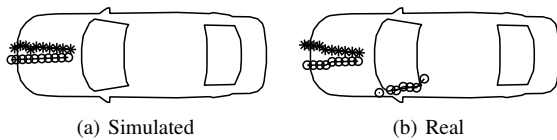


Fig. 16. Real and simulated data in situation 3

Finally, Fig. 17 shows a single snapshot of a situation that our simulation is not yet capable to reproduce correctly. Observer and target vehicle are standing still with a distance of about 1m. While the front plane reflector model is approved again by the detections on the left, in the real data there are a number of additional detections. These occur because the radar energy that propagates more than once between object and observing vehicle (multiple back-and-forth reflections) is still strong enough to cause detections.

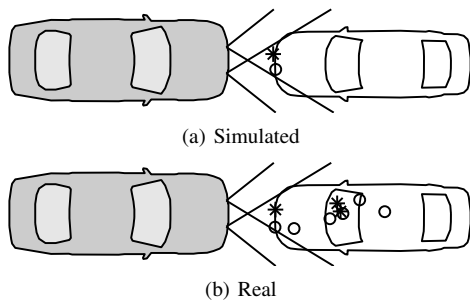


Fig. 17. Real and simulated data in situation 4

VI. OUTLOOK AND FURTHER WORK

The simulation in its current state is able to generate realistic radar targets lists in the majority of scenarios. By considering some additional effects, the range of possible scenarios can even be expanded.

We have mentioned before that in situations where the distance between radar sensor and object is very small, additional detections are caused by multiple back-and-forth reflections. This effect can be modeled by adding duplicates of existing reflection centers at integer multiples of the measured distance.

Further, a multipath propagation and interference model could be added to enhance the radar amplitude simulation. If the amplitude is only of secondary importance in the consecutive processing algorithms, the current solution is sufficient.

The presented real data sets were recorded in a test site free of any disturbing obstacles, thus misdetections were very rare. In other environments, however, there will be more misdetections due to numerous small reflectors or multiple reflections between different obstacles. As the target list processing algorithms have to cope with those spurious targets, they should also appear in simulated target lists. For the algorithms it will not be important how exactly a misdetection occurred, thus it will be sufficient to add misdetections randomly instead of adding, for example, a sophisticated ray-tracing model for multiple reflections between objects.

VII. CONCLUSION

We have presented a new simulation principle for automotive radar target lists. By limiting the intended application area of the simulation to the development of target list processing algorithms, we were able to significantly reduce the programming effort as well as the computational load in comparison to a finite-element-like simulation.

Vehicles and obstacles are represented by a small number of point reflection centers and plane reflectors, which are parametrized with aid of a moderate amount of real measurement data. A geometrically computed ideal target list is turned into a realistic one by applying a simplified sensor model and adding artificial noise in different stages.

As we have shown by the results of our simulation, not every detail about the sensor internals is necessary to build a realistic sensor model and to simulate a realistic radar target list. Even if not every physical effect is considered, the simulation is a valuable tool for the development of radar signal processing algorithms.

ACKNOWLEDGMENT

This work was kindly supported by Dirk Linzmeier and Michael Skutek of the DaimlerChrysler AG by providing the opportunity to record the necessary radar measurement data.

REFERENCES

- [1] Hermann Henftling, Dirk Klotzbücher, and Christian Frank, "Ultra wide band 24GHz sequential lobing radar for automotive applications," in *Proc. Intern. Radar Symposium (IRS)*, Berlin, Germany, Sept. 2005.
- [2] Constantine A. Balanis, *Antenna Theory*, John Wiley & Sons, New York, NY, 1982.
- [3] Samuel S. Blackman, *Multiple-Target Tracking with Radar Applications*, Artech House, 1986.
- [4] Rainer Wiedemann, *Simulation des Straßenverkehrsflusses*, Schriftenreihe des Instituts für Verkehrswesen der Universität Karlsruhe, Heft 8, 1974.
- [5] P. G. Gipps, "A model for the structure of lane-changing decisions," *Transportation Research*, vol. 20B, no. 5, pp. 403–414, 1986.